Kuang Xingxing (Orcid ID: 0000-0001-6375-617X)

Tetzlaff Doerthe (Orcid ID: 0000-0002-7183-8674)

Using stable isotopes of surface water and groundwater to quantify moisture sources across the Yellow River source region

Xingxing Kuang[1], Xin Luo[2,3], Jiu Jimmy Jiao[2,3*], Sihai Liang[4], Xiaolang Zhang[1,2], Hailong Li[1], Junguo Liu[1]

[1] Guangdong Provincial Key Laboratory of Soil and Groundwater Pollution Control, School of Environmental Science and Engineering, Southern University of Science and Technology, Shenzhen 518055, China

[2] Department of Earth Sciences, The University of Hong Kong, Pokfulam Road, Hong Kong, China

[3] The University of Hong Kong, Shenzhen Research Institute (SRI), Shenzhen, China

[4] School of Water Resources and Environment, China University of Geosciences, Beijing, China

[*] Corresponding author: Tel: +852 2857 8246; Fax: +852 2517 6912; E-mail: jjiao@hku.hk

This article has been accepted for publication and undergone full peer review but has not been through the copyediting, typesetting, pagination and proofreading process which may lead to differences between this version and the Version of Record. Please cite this article as doi: 10.1002/hyp.13441

Running title: Stable isotopes of water across Yellow River source region

Abstract

Characterization of stable isotope compositions (δ^2H and $\delta^{18}O$) of surface water and groundwater in a catchment is critical for refining moisture sources and establishing modern isotope-elevation relationships for paleoelevation reconstructions. There is no consensus on the moisture sources of precipitation in the Yellow River source region during summer season. This study presents δ^2H and $\delta^{18}O$ data from 111 water samples collected from tributaries, mainstream, lakes, and groundwater across the Yellow River source region during summertime. Measured $\delta^{18}O$ values of the tributaries range from -13.5‰ to -5.8‰ with an average of -11.0‰. Measured $\delta^{18}O$ values of the groundwater samples range from -12.7‰ to -10.5‰ with an average of -11.9‰. The $\delta^{18}O$ data of tributary waters display a northward increase of 1.66‰ per degree latitude. The $\delta^{18}O$ data and d-excess values imply that moisture sources of the Yellow River source region during summertime are mainly from the mixing of the Indian Summer Monsoon and the Westerlies, local water recycling, and subcloud evaporation. Analysis of tributary $\delta^{18}O$ data from the Yellow River source region and streamwater and precipitation $\delta^{18}O$ data from its surrounding areas leads to a best-fit second-order polynomial relationship between $\delta^{18}O$ and elevation over a 4600 m elevation

range. A $\delta^{18}O$ elevation gradient of -1.6‰/km is also established using these data and the gradient is in consistence with the $\delta^{18}O$ elevation gradient of north and eastern plateau. Such relationships can be used for paleoelevation reconstructions in the Yellow River source region.

Keywords: river water, groundwater, lake water, precipitation, moisture source, paleoelevation, Indian Summer Monsoon, Tibetan Plateau

1 INTRODUCTION

Isotopic composition of precipitation provides a conservative tracer for the origin, transport, and phase transitions of water in the water cycle (Dansgaard, 1964; Gat, 1996; Rozanski, Araguás-Araguás, & Gonfiantini, 1993). Variations in isotopic composition of precipitation are mainly controlled by atmospheric parameters such as temperature, relative humidity, and evaporation (Dansgaard, 1964; Rozanski et al., 1993; Yurtsever & Gat, 1981), and by geographic parameters such as altitude, latitude, and distance inland (Craig, 1961; Gat, 1996; Karim & Veizer, 2002; Kendall & Coplen, 2001; Siegenthaler & Oeschger, 1980). Stream waters can provide an integrated representation of the isotopic composition of precipitation in the drainage basin above the sample elevation (Rowley & Currie, 2006; Rowley & Garzione, 2007). They are better representation of monthly or annual weighted averages than individual precipitation events (Kendall & Coplen, 2001). Stream waters collected from small catchments do indeed reflect the average isotopic composition of precipitation (Hoke, Jing, Hren, Wissink, & Garzione, 2014; Hren, Bookhagen, Blisniuk, Booth, & Chamberlain, 2009; Li & Garzione, 2017). Stable isotopes of modern water are frequently used to identify moisture sources and moisture transport pathways on the Tibetan Plateau (Bershaw, Penny, & Garzione, 2012; Hren et al., 2009; Li & Garzione, 2017; Ren, Yao, & Xie, 2017a; Ren, Yao, Xie, & He, 2017b; Tian, Masson-Delmotte, Stievenard, Yao, & Jouzel, 2001a; Tian et al., 2007; Weynell, Wiechert, & Zhang, 2016; Xu et al., 2014).

Summer precipitation on the southern and eastern Tibetan Plateau is mainly controlled by the Indian Summer Monsoon and/or East Asian Summer Monsoon (Bershaw et al., 2012; Tian et al., 2007; Liu, Tian, Chai, & Yao, 2008; Xu et al., 2014), as shown in Figure 1. Precipitation on the southern Tibetan Plateau has been found to be dominated by the Indian Summer Monsoon (Hren et al., 2009; Li & Garzione, 2017; Ren et al., 2017b; Tian et al., 2001a; Yao et al., 2013). Previous studies show that the maximum northward extent of the Indian Summer Monsoon is about 33-35ºN (Araguás-Araguás, Froehlich, & Rozanski, 1998; Tian et al., 2007). The maximum westward extent of the Indian Summer Monsoon lies in the range between 85 and 87ºE (Hren et al., 2009). Beyond north of about 30ºN the role of the Indian Summer Monsoon starts to decrease and the dominant moisture sources changes (Hren et al., 2009). Yao, Zhou, & Yang (2009) pointed out that the plateau can be divided into three zones: the monsoon zone (south of 30 °N), the transition zone (between 30 and 35 °N), and the westerly zone (north of 35 °N). Moisture in the transition zone is provided by part of the monsoon and part of continental water recycling (Yao et al., 2009). In the middle part of the Tibetan Plateau, local recycling plays an important role in the hydrological cycle (Tian et al., 2001a; Tian, Yao, Sun, Stievenard, & Jouzel, 2001b; Tian et al., 2003; Tian et al., 2008; Yao et al., 2013). Simulated results indicate that in summer more than 50% of the precipitation is provided by continental recycling (Koster, de Valpine, & Jouzel, 1993). Precipitation on the eastern Tibetan Plateau is mainly controlled by the East Asian Summer Monsoon (Lan et al., 2010b; Xu et al., 2014). Lan et al. (2010b) point out that the moisture in the Yellow River source region is transported from the western Pacific Ocean. On the basis of chemical and isotopic composition of surface waters in the catchment of Lake Donggi Cona (north to the Yellow River source region), Weynell et al. (2016) found that moisture in this region is related to the East Asian Summer Monsoon. Xu et al. (2014) found that precipitation across the Longmenshan margin (eastern Tibetan Plateau) is dominated by the East Asian Summer Monsoon.

Moisture of the Yellow River source region has been found to be derived from different sources including the East Asian Summer Monsoon, the Indian Summer Monsoon, and the Westerlies (Bolch et al., 2012; Liu et al., 2008; Song, Huang, Richards, Ke, & Phan, 2014; Weynell et al., 2016; Yao et al., 2012; Yao et al., 2013). Researchers pointed out that precipitation in the wet season (June–September) is caused by the southwest monsoon from the Bay of Bengal in the Indian Ocean, i.e., the Indian Summer Monsoon (Hu, Maskey, Uhlenbrook, & Zhao, 2011; Hu, Maskey, & Uhlenbrook, 2013a; Zheng et al., 2009). However, other researchers pointed out that the climate in the Yellow River source region is strongly governed by the East Asian Summer Monsoon, which brings warm and wet air in the summer (Hu, Maskey, & Uhlenbrook, 2013b; Lan et al., 2010b; Yang, Ding, Chen, Liu, & Lu, 2003). On the basis of previous studies, the Yellow River source region is both the maximum northward extent of the Indian Summer Monsoon (Tian et al., 2007; Yao et al., 2009) and the maximum westward extent of the East Asian Summer Monsoon (Araguás-Araguás et al., 1998; Johnson & Ingram, 2004). Currently, there is no consensus about the moisture source of the region during summer season.

Surface rainfall and surface water isotopic compositions have frequently been used for stable isotope-based approaches to paleoelevation reconstructions. The paleoelevation of a catchment can be calculated from the measured stable isotope compositions using empirical isotope-elevation lapse rates (Garzione, Dettman, Quade, DeCelles, & Butler, 2000a; Garzione, Quade, DeCelles, & English, 2000b; Poage & Chamberlain, 2001) or thermodynamic Rayleigh-distillation elevation-isotope models (Rowley, Pierrehumbert, & Currie, 2001; Rowley, 2007; Rowley & Garzione, 2007). Stable isotopes have recently been applied in a number of paleoelevation studies in the Himalaya and Tibetan Plateau (Currie, Rowley, & Tabor, 2005; Cyr, Currie, & Rowley, 2005; Garzione et al., 2000a, 2000b; Hoke et al., 2014; Li & Garzione, 2017; Quade, Breecker, Daëron, & Eiler, 2011; Ren et al., 2017b; Rowley et al., 2001; Rowley & Currie, 2006). For example, on the basis of stable isotopes of the tributaries of the Mekong River, Hoke et al. (2014) found that the southeast Tibetan Plateau margin has been at or near their present elevation during the Eocene and Neogene. Although many studies on paleoelevation reconstructions have been conducted on different parts of the Tibetan Plateau as indicated above, there are very limited studies on paleoelevation reconstructions in the Yellow River source region.

The δ^2H and $\delta^{18}O$ characteristics of the Yellow River source region may be complicated by interactions of the monsoons and continental recycling. Ren, Yao, Yang, & Joswiak (2013) analyzed δ^2H and $\delta^{18}O$ of rain and snow samples at Madoi (northwest Yellow River source region) and found that precipitation in the region is significantly influenced by summer monsoon and probably by local moisture recycling. It is important to investigate the characteristics of the stable isotopes of surface water and groundwater of this region to identify the moisture sources. However, studies on stable isotopes of the Yellow River source region are very limited. In this paper, we present stable isotope data ($\delta^{18}O$ and δ^2H) from modern surface water and groundwater across the Yellow River source region. The objectives of this paper is to use the isotopic data to refine moisture sources of the region and define isotope-elevation relationships for paleoelevation reconstructions. This is the first study that focuses solely on the Yellow River source region to investigate moisture sources and paleoaltimetry.

2 STUDY AREA

The Yellow River source region, located on the eastern Tibetan Plateau, refers to the area between 95°50'45" –103°28'9" E and 32°12'11"–35°48'7" N (Zheng, Zhang, Liu, Shao, & Fukushima, 2007). The Tangnag hydrological station has been generally used as the outlet of the catchment (Figure 1). The region is bounded by the Bayankala Mountains in the south, the Buqing Mountains in the north, and the Yueguzonglie highland in the west (Liang, Ge, Wan, & Zhang, 2010; Wang, Wang, Li, Wu, & Yang, 2015). It covers an area of 121 972 km^2 and the river length in the source region is about 1553 km (Zhen et al., 2007). The annual mean runoff is 2.05×10^{10} m^3 yr^{-1}, which accounts for 35% of the total runoff of the Yellow River (Lan et al., 2010b; Zheng et al., 2007). Therefore, the region is called the "water tower" of the Yellow River (Hu et al., 2011; Zheng et al., 2007, 2009; Zhou & Huang, 2012). The altitude of the area decreases from west to east with the highest elevation (6282 m) in the Animaqing Mountains and the lowest elevation (2546 m) in the Tangnag village (Figure 1).

For most of the area, the altitude is between 3480 and 4680 m above sea level. Large areas of this region are covered by grassland, lakes, and swamps. About 80% of this area is covered by grassland. There were about 5300 lakes with a total area of 2000 km^2 in the source region in the 1980s (Hu et al., 2011; Liang et al., 2010). The largest two lakes in the area are the Zhaling Lake and Eling Lake, each covers an area of 526 km^2 and 611 km^2 (Liang et al., 2010). The Yellow River flows through these two fresh water lakes. Human activities in the region are limited (Hu et al., 2011; Zheng et al., 2009). The population density of this region is about 0.34 person/km^2 (Liang et al., 2010). The influence of human activities on runoff is insignificant and variations in streamflow should be mainly controlled by meteorological factors (Sato et al., 2008).

The climate of the Yellow River source region is cold and semiarid or semi-humid with short warm and long cold seasons, which is the typical Tibetan Plateau climate system (Hu et al., 2011; Wang et al., 2015; Zheng et al., 2007). The annual mean air temperature varies from –4 to 2 ^{o}C from northwest to southeast. According to the monthly mean air temperature from 1960 to 2000, the warmest month is July and the corresponding mean daily air temperature is around 8 ^{o}C. The air temperature is well below 0 ^{o}C from October to April. Precipitation in the region decreases from southeast to northwest (Figure 1). The amount of mean annual precipitation decreases from about 800 mm in the southeast to about 300 mm in the northwest (Meng, Su, Yang, Tong, & Hao, 2016; You, Min, Zhang, Pepin, & Kang, 2015; Zhou & Huang, 2012). The regional annual mean precipitation is about 534 mm. Up to 75–90% of the annual precipitation falls in the wet season from June to September with a peak in July (Hu et al., 2011, 2013a; Zheng et al., 2009). Snowfall in the region occurs mainly from November to

March and the total amount of annual snowfall is less than 10% of the annual precipitation (Hu et al., 2011).

Permanent snowpacks and glaciers are mainly distributed in the Animaqing and Bayankala Mountains (Zheng et al., 2007). There are 58 glaciers with a total area of about 125 km^2 on the eastern slope of the Animaqing Mountains, accounting for 96% of the total area of glaciers in the region (Yang et al., 2003). The total glacier area in the Yellow River source region is about 134 km^2, which occupies only about 0.11% of the drainage basin (Zhang, Su, Yang, Hao, & Tong, 2013). Permafrost is present in most of the area and the remaining area is covered by seasonal frozen ground (Cheng & Wu, 2007).

Runoff in the Yellow River source region is mainly controlled by precipitation (Hu et al., 2011; Lan, Kang, Ma, Yang, & Yao, 1999; Li et al., 1999; Yang, Ding, & Chen, 2007a). Seasonal fluctuations in runoff in this region is similar to that of precipitation. On the basis of observed discharge data at Tangnag hydrological station from 1960 to 2000, runoff also shows a peak in July (Sato et al., 2008). About 70% of the annual total runoff is distributed from June to October (Hu et al., 2011). There are four hydrological stations in the source region: Madoi, Jimai, Maqu, and Tangnag (Figure 1). The mean annual runoff at Madoi is 4.41×10^8 m^3 yr^{-1} (Zhang, Li, & Liang, 2012) which is less than 5% of the total flow at Tangnag. Rainfall runoff, groundwater, and ice and snow melt water has been found to accounts for 63.5%, 26.8%, and 9.7% of the normal annual flow, respectively (Lan et al., 2010a). Hence the runoff is mainly derived from precipitation in summer and autumn, and groundwater and melt water only play a secondary role (Lan et al., 2010a).

3 SAMPLING AND ANALYSIS

Water samples were collected from August 18 to September 3 of 2015 across the Yellow River source region. Samples were collected from the mainstream, tributaries, lakes, and groundwater. Locations of the sample sites are shown in Figure 1. Elevations of sampling sites range from 2186 m northeast of the region to 4490 m in the central of the region near the Animaqing Mountains (Appendix A Table 1). A total of 111 samples were collected, including 67 river water samples (38 tributaries and 29 mainstream samples), 31 lake water samples, and 13 groundwater samples. Groundwater samples were taken from lakeshore aquifers and river banks using a pushpoint sampler (M.H.E.) with a peristaltic pump (Solinst). Groundwater samples were also collected from wells near the Zhaling and Eling lakes.

The time of field sampling belongs to the wet season of the source region. During the field sampling work, there was no significant precipitation event. Waters in the river channels are assumed to reflect summertime integrated rainfall and groundwater composition (e.g., Bershaw et al., 2012; Hren et al., 2009; Kendall & Coplen, 2001; Ren et al., 2017a; Tian et al., 2001a). The field data were collected in one single season, it is possible that the interannual changes of stable isotopic compositions may bias the observations of stable isotopic characteristics. However, previous studies on stable isotopes in surrounding areas show minor interannual changes (e.g., Hren et al., 2009; Hoke et al., 2014). In addition, Ren et al. (2013) show that $\delta^{18}O$ values of precipitation in August and September are close to the seasonal average $\delta^{18}O$ value.

The samples were filtered with 0.45 μm filters (Advantec) in situ and taken into 2 mL Nalgene centrifugation tubes for $\delta^{2}H$ and $\delta^{18}O$ analysis. The samples were stored and transported in darkness and refrigerated in the laboratory prior to analysis. δ^2H and $\delta^{18}O$ were measured with MOA-ICOS laser absorption spectrometer (Los Gatos Research (LGR) Triple Isotope Water Analyzer (TIWA-45EP)) at State Key Laboratory of Marine Geology, Tongji University, Shanghai. The measurement uncertainty is better than ±0.1‰ for $\delta^{18}O$ and ±0.5‰ for δ^2H, respectively. The isotopic compositions of the waters are reported in permil (‰) relative to the Vienna Standard Mean Ocean Water (VSMOW).

4 RESULTS

4.1 $\delta^{18}O$ and δ^2H of surface water and groundwater

Measured $\delta^{18}O$ values of the mainstream range from -11.3‰ to -3.6‰ with an average of -9.7‰, and δ^2H values range from -82.3‰ to -34.3‰ with an average of -73.4‰ (Appendix A Table 1). Measured $\delta^{18}O$ values of the tributaries range from -13.5‰ to -5.8‰ with an average of -11.0‰, and δ^2H values range from -95.7‰ to -46.5‰ with an average of -78.8‰ (Appendix A Table 1). The relationship between δ^2H and $\delta^{18}O$ of the river waters is shown in Figure 2. $\delta^{18}O$ of most of the river water samples falls between -14‰ and -8‰. There are four mainstream samples have $\delta^{18}O$ values higher than -8‰. In addition, there is only one tributary sample has $\delta^{18}O$ value higher than -8‰.

Samples from the lakes in the region are characterized by extremely enriched isotopic compositions except for the Ximen Co (Appendix A Table 1). Measured $\delta^{18}O$ values of the lakes range from -4.1‰ to -0.7‰ with an average of -2.8‰. Measured δ^2H values range from -38.3‰ to -21.7‰ with an average of -31.2‰ at these same localities. Figure 2 shows that $\delta^{18}O$ of most of the lake samples are higher than -4‰. For the Ximen Co, the measured $\delta^{18}O$

of the lake waters range from -13.4‰ to -12.1‰ with an average of -12.5‰, and δ^2H values range from -93.2‰ to -87.1‰ with an average of -89.1‰.

Measured $\delta^{18}O$ values of the groundwater range from -12.7‰ to -10.5‰ with an average of -11.9‰, and δ^2H values range from -91.3‰ to -80.1‰ with an average of -85.8‰ (Appendix A Table 1). The average $\delta^{18}O$ of the groundwater samples is close to that of the tributaries.

The stable isotopic data from the tributaries are fitted to a line by linear regression as $\delta^2\mathrm{H} = 6.45\delta^{18}\mathrm{O} - 7.68$ ($R^2 = 0.92$), as shown in Figure 2. A close examination of Figure 2 shows that isotope data with $\delta^{18}O$ lower than -8‰ fall closely about the global meteoric water line (GMWL) $\delta^2\mathrm{H} = 8\delta^{18}\mathrm{O} + 10$ (Craig, 1961). The isotopic data for the groundwater samples all fall closely to the intersection point of the GMWL and the fitted line. As the intersection point indicates the original water (Clark & Fritz, 1997), the isotopic composition of groundwater is close to that of the original water in the Yellow River source region.

The $\delta^{18}O$ values of the tributaries are negatively related to the annual precipitation across the area (Figure 3). The annual precipitation was obtained based on the mean annual precipitation contours presented by Meng et al. (2016). Although the data points are relatively scattered, a negative correlation can be seen. Sites with larger annual precipitation show more deleted $\delta^{18}O$ values, while sites with smaller annual precipitation show more enriched $\delta^{18}O$ values.

4.2 Spatial distribution of δ^{18}O and δ^2H values

Different kinds of waters in the region show different spatial patterns. Most of the data points for the mainstream are concentrated on the -11‰ level from south to north except four data points which have $\delta^{18}O$ values higher than -8‰ (Figure 4a). The four points all located in the northwest part of the source region and downstream of the Zhaling Lake and Eling Lake. The $\delta^{18}O$ values of the two lakes are very enriched due to evaporation. The four points with enriched $\delta^{18}O$ values are likely due to the fact that they receive water from the two lakes. On the other hand, $\delta^{18}O$ of the mainstream decreases from west to east but the decreasing rate changes at about 99ºE (Figure 4b). $\delta^{18}O$ values of the mainstream samples decrease monotonously from west to east with longitude greater than about 99ºE.

For the tributaries, $\delta^{18}O$ values become progressively enriched from south to north (Figure 4a). On the other hand, the $\delta^{18}O$ values of the tributaries show an overall decreasing trend from west to east (Figure 4b). Although an overall decreasing trend, $\delta^{18}O$ values of the tributaries show an increasing trend east of about 99ºE. A linear relationship between $\delta^{18}O$ and latitude can be found, as shown in Figure 5a. The $\delta^{18}O$ values increase by 1.66‰ per degree latitude northward across the region. This increasing rate is similar to previous studies using transects across the Tibetan Plateau. An increasing rate of about 1.5‰ was obtained from both transects of eastern plateau and central plateau (Bershaw et al., 2012; Quade et al., 2011). There is only one sample with $\delta^{18}O$ value significantly higher than others. The high $\delta^{18}O$ value is possibly due to evaporation. A linear relationship can also be defined for the relationship between $\delta^{18}O$ and longitude (Figure 5b). Compared with Figure 5a, the linear relationship between $\delta^{18}O$ and longitude is relatively weak. The uniquely high $\delta^{18}O$ value also does not seem to represent the regional trend and is not included in the regression.

The spatial distribution of $\delta^{18}O$ values of the tributaries is shown in Figure 6. Tributaries in the central and southeast parts have $\delta^{18}O$ values ranging from -13‰ to -11‰. In the northwest part, samples collected from tributaries surrounding the two largest lakes show relatively enriched $\delta^{18}O$ values. The measured $\delta^{18}O$ values of these samples range from -10.6‰ to -5.8‰ with most of the tributaries have $\delta^{18}O$ values higher than -10‰. These relatively enriched $\delta^{18}O$ values indicate a certain extent of evaporation. Such a spatial pattern indicates that wet region (central and southeast parts) of the source region has more depleted $\delta^{18}O$ values while dry region (northwest part) has more enriched $\delta^{18}O$ values.

Lakes in northwest and southeast of the region show distinct difference in isotopic compositions (Figure 4). Lakes in the northwest part show significantly enriched isotopic compositions while lakes in the southeast part show significantly depleted isotopic compositions. For the Ximen Co, as it is located in the southeast part and dominantly recharged from snow and glacier melting (Luo et al., 2018), the $\delta^{18}O$ and $\delta^{2}H$ values are much lower than those of the Zhaling Lake and Eling Lake. For open lakes such as the Zhaling Lake, Eling Lake, and Ximen Co, the evaporative enrichment in isotopic composition also depends on the water residential time. As the Zhaling and Eling Lakes are significantly larger than Ximen Co, water residence time in the two lakes are much longer than that of Ximen Co.

For the groundwater samples, Figure 4 shows that the $\delta^{18}O$ values concentrated around -12‰. As mentioned earlier, the average $\delta^{18}O$ value of the groundwater samples is -11.9‰. The $\delta^{18}O$ values of groundwater samples are very close to each other, no matter where the sample was collected. There is no apparent difference between $\delta^{18}O$ values of groundwater samples collected from the northwest and southeast parts of the source region.

4.3 Spatial distribution of d-excess

Deuterium excess was defined by Dansgaard (1964) as $\text{d-excess} = \delta^2\text{H} - 8\delta^{18}\text{O}$. The global average d-excess in precipitation was found to be close to 10‰. Water vapor derived from the eastern Mediterranean Sea has significantly higher d-excess values (>20‰) than water vapor derived from Pacific or Indian Oceans (about 10‰) (Gat & Carmi, 1970). This parameter has been found to be the most useful stable isotope property for characterizing the water vapor origin (Gat & Carmi, 1970). The d-excess values show a great variety across the Yellow River source region. Different water bodies in the region have significantly different d-excess values (Figure 7). The d-excess of the mainstream ranges from -9.9‰ to 11.4‰ with an average of 4.6‰ (Appendix A Table 1). The d-excess of the tributaries ranges from -0.4‰ to 16.3‰ with an average of 9.5‰. The d-excess of groundwater ranges from 3.9‰ to 11.8‰ with an average of 9.1‰. The average d-excess values of the tributaries and groundwater are very similar to each other. Lakes in the northwest and southeast parts of the region have distinctly different d-excess values. For lakes in the southeast part, the d-excess values range from 9.0‰ to 14.4‰ with an average of 10.8‰. For lakes in the northwest part, all the lakes show negative d-excess values. The two largest lakes, Zhaling Lake and Eling Lake, have d-excess values significantly different from other lakes in this region. The d-excess values for the two lakes range from -5.5‰ to -10.2‰ with an average of -6.8‰. The d-excess values for other lakes in this area range from -11.9‰ to -16.2‰ with an average of -13.7‰.

The d-excess values of the tributaries show a wide range of variety and do not show a notable pattern of spatial distribution (Figure 8). Although the average d-excess value of the tributaries is around 10‰, the d-excess values of different tributaries fluctuate significantly across the region. The extremely low d-excess values are mainly distributed in the northwest part of the region. Even in the northwest part, the d-excess values also show a wide range of variety. The d-excess values in the northwest part range from -0.4‰ to 13.8‰. The d-excess values in the central and southeast parts are relatively high and many sites have d-excess values close to 10‰. Overall, there is no apparent relationship between d-excess and latitude (Figure 7a) and longitude (Figure 7b) across the region.

5 DISCUSSION

5.1 Implications for moisture source

In the Yellow River source region, the $\delta^{18}O$ values show a significant south-north gradient of 1.66‰ per degree latitude (Figure 5a). The general south-north gradient across the entire source region can also be seen in Figure 6. The increasing of $\delta^{18}O$ northward is in consistent with previous studies (Bershaw et al., 2012; Caves et al., 2015; Hren et al., 2009; Li & Garzione, 2017). The increasing rate is also very close to that obtained from transects northward across the eastern and central plateau (1.5‰ per degree latitude), as given by Bershaw et al. (2012) and Quade et al. (2011). Such a south-north gradient north than 30ºN has been attributed to increased mixing between southerly moisture from the Indian Summer Monsoon and $\delta^{18}O$-enriched moisture from the mid-latitude Westerlies (Bershaw et al., 2012; Caves et al., 2015; Hren et al., 2009; Li & Garzione, 2017; Quade et al., 2011; Yao et al., 2013). This mixing of Indian Summer Monsoon and Westerlies is also supported by studies on water vapour flux over the Tibetan Plateau (Chen et al., 2012; Curio et al., 2015; Feng & Zhou, 2012). The significant south-north gradient of $\delta^{18}O$ in the Yellow River source region also indicates that the moistures sources are mainly the mixing of the Indian Summer Monsoon and the Westerlies.

The $\delta^{18}O$ values of the Yellow River source region do not show an obvious east-west trend (Figures 5b and 6). Although a linear relationship can be obtained, the R^2 value is quite low (R^2=0.16). The $\delta^{18}O$ values show a minimum around 99ºE and then an increasing trend eastern of 99ºE. The $\delta^{18}O$ data show a decreasing trend west of 99ºE (Figure 5b). Even in the region west of 99ºE, precipitation from the evaporation of the Zhaling Lake and Eling Lake may contribute to the enriched $\delta^{18}O$ values of the tributaries surrounding the two lakes (Figure 6). Waters in the two lakes show enriched isotopic compositions, as can be seen in Figure 2 and Appendix A Table 1. As a result, the west-east decreasing trend may not be treated as a trend induced by moisture source from the west or the east.

On the basis of the above analysis, the contribution of the East Asian Summer Monsoon to precipitation on the Yellow River source region should be limited. This conclusion is in consistence with previous studies on moisture sources of surrounding areas. Li and Garzione (2017) found that the East Asian Summer Monsoon is not the major source of moisture to the eastern plateau due to the lack of east-west $\delta^{18}O$ gradients. The eastern-most part of the plateau was found to be the limit of influence of the East Asian Summer Monsoon (Bershaw et al., 2012; Li & Garzione, 2017). Previous studies on moisture flux and wind vectors over the Tibetan Plateau during summertime also supported the limited contribution of the East Asian Summer Monsoon (Chen, Xu, Yang, & Zhang, 2012; Curio et al., 2015; Ren et al., 2017b).

The relatively high d-excess values (>10‰) across the region possibly indicate local moisture recycling exists across the whole region (Figure 8). This finding is also in consistence with results obtained by analyzing δ^2H and δ^{18}O of rain and snow samples at Madoi (Ren et al., 2013). Previous studies show that local moisture recycling is an important process affecting precipitation over the Tibetan Plateau (Bershaw et al., 2012; Hren et al., 2009; Kurita & Yamada, 2008; Li & Garzione, 2017; Tian et al., 2001a, 2001b, 2003, 2008; Yao et al., 2013). About 47% to 73% of precipitation was found to be provided by recycling in the inner Tibetan Plateau (Curio et al., 2015; Koster et al., 1993; Yang, Yao, Wang, Tian, & Gou, 2006; Yang, Yao, Gou, & Tang, 2007b).

Subcloud evaporation should also be one of the sources of moisture across the Yellow River source region. Previous studies show that subcloud evaporation of raindrops decreases d-excess and local moisture recycling increases the d-excess value (Fröhlich, Gibson, & Aggarwal, 2001; Froehlich et al., 2008; Gat 1996; Guan, Zhang, Skrzypek, Sun, & Xu, 2013; Li & Garzione, 2017; Rozanski et al., 1993). The relatively high δ^{18}O but low d-excess in the northeastern and northwestern of the source region are probably represent subcloud evaporation of rainfall due to the low precipitation amount (Froehlich et al., 2008; Li & Garzione, 2017; Ren et al., 2017a, 2017b; Xu et al., 2014). The d-excess values of both the tributaries and groundwater samples in these two parts are relatively low compared with those of other parts of the region.

In general, the isotopic composition of groundwater closely reflects the average annual isotopic composition of local precipitation (Fritz, 1981). Ren et al. (2013) found that the amount-weighted averaged $\delta^{18}O$ and $\delta^{2}H$ for all precipitation events at Madoi during May 2009 to April 2010 are -12.2‰ and -86.4‰, respectively. The average $\delta^{18}O$ and $\delta^{2}H$ of the groundwater samples are very close to those of Ren et al. (2013). As indicated earlier, the $\delta^{18}O$ values of groundwater samples are very close to each other across the region. The relatively uniform stable isotope compositions of groundwater across the region may imply that the moisture sources across the region are similar.

In summary, moisture sources of the Yellow River source region during the wet season are from multiple sources including the mixing of the Indian Summer Monsoon and the Westerlies, local water recycling, and subcloud evaporation. The East Asian Summer Monsoon plays a limited role in providing moisture to precipitation in this region. This finding is different from previous studies which pointed out that moisture of the region is transported either by the Indian Summer Monsoon or the East Asian Summer Monsoon.

5.2 Implications for paleoelevation reconstructions

The relationship between $\delta^{18}O$ of tributary streamwater and basin mean elevation in the study area is investigated for paleoelevation reconstructions. In addition to the tributary water samples from the Yellow River source region, streamwater $\delta^{18}O$ data from Siang Zangbo Basin (94.77°–95.20°E and 28.14°–28.78°N) by Hren et al. (2009) and GNIP data from New Delhi (77.20°E, 28.58°N), Shilong (91.88°E, 25.57°N), and Yangoon (96.17°E, 16.77°N) by Ren et al. (2017b) were also collected. A least squares analysis of the elevation versus $\delta^{18}O$ data yields the second order polynomial relationship $z = -34.818(\delta^{18}\mathrm{O})^2 - 1197.4(\delta^{18}\mathrm{O}) - 4981.9$ ($R^2 = 0.96$), where z is elevation above sea level (m), which is shown in Figure 9a. Nine samples were not included in the least squares analysis because they do not seem to represent the general trend. The nine samples are all located in the northwest part of the region (i.e., west of 98ºE), as can be seen in Figure 6.

The x-intercept of this polynomial fit is about -4.8‰ at zero elevation. Based on this x-intercept value at zero elevation, a linear fit is also obtained as $z = -619.18(\delta^{18}\mathrm{O}) - 2972.06$ ($R^2 = 0.93$). The linear fit leads to a δ^{18}O elevation gradient of -1.6‰/km. The fitted elevation gradient is very close to the δ^{18}O elevation gradient of -1.5‰/km on the northern and eastern parts of the Tibetan Plateau (Ding et al., 2009; Quade et al., 2007; Xu et al., 2014).

A comparison of different δ^{18}O-elevation relationships on the southeastern and eastern Tibetan Plateau is shown in Figure 9b. These relationships are obtained from tributaries of the Yarlung Zangbo River in the southeastern Tibetan Plateau (Hren et al., 2009; Ren et al., 2017b), tributaries of the Lancang River (Hoke et al., 2014), and streams along the eastern Tibetan Plateau (Xu et al., 2014). Among these models, one is a thermodynamic model (Hren et al., 2009) and others are second order least squares polynomial relationships (Hoke et al., 2014; Ren et al., 2017b; Xu et al., 2014). Figure 9b shows that the two relationships from the southeastern Tibetan Plateau are close to that of this study. Both of them are almost all located in the 95% confidence interval of the current relationship. The other two models are relatively far from the model of this study. The δ^{18}O values of different relationships at zero elevation are quite different from each other.

This study constructs δ^{18}O-elevation relationships over a 4600 m elevation range for the Yellow River source region and surrounding areas. Both the second-order polynomial relationship and the linear relationship can be used to predict elevation if $\delta^{18}O$ value is known. The polynomial relationship shows a slightly better agreement with the measured data than the linear relationship. A comparison of predicted elevation with the basin mean elevation is shown in Appendix A Table 2. The differences between predicted elevation using the polynomial relationship and the basin mean elevation range from -322 m to 577 m. The differences between predicted elevation using the linear relationship and the basin mean elevation range from -811 to 962 m. The differences for the polynomial relationship are smaller than those of the linear relationship. In reconstructing paleoelevation of the Yellow River source region, the polynomial relationship is better than the linear relationship to represent the elevation effect. In addition, samples east of about 98ºE are preferred as samples from west of 98ºE are more complex to interpret and should be used with caution. Paleoelevation reconstructions using $\delta^{18}O$ data west of 98ºE may lead to higher uncertainties.

6 CONCLUSIONS

Stable isotopic compositions of modern surface waters and groundwater across the Yellow River source region are used to investigate moisture sources to this region and build relationships between $\delta^{18}O$ and elevation for paleoelevation reconstructions. A total of 111 water samples from mainstream, tributary, lakes, and groundwater were collected and stable isotopic compositions of these samples are presented. The stable isotopic characteristics of the river water, lake water, and groundwater are identified based on the measured data. Northward across the source region, there is a positive trend in tributary water $\delta^{18}O$ with latitude (1.66‰ per degree latitude). The stable isotopic compositions of groundwater across the region are vary similar to each other and the mean $\delta^{18}O$ value is close to that of the tributary waters. Lakes in the northwest part of the region are characterized by extremely enriched isotopic compositions. Such enriched isotopic compositions show significant evaporation of the lakes.

The $\delta^{18}O$ and d-excess values indicate that external moisture sources to the Yellow River source region during summertime are mainly the Indian Summer Monsoon and the Westerlies. Local moisture recycling and subcloud evaporation also paly an important role in precipitation in the region. The contribution of the East Asian Summer Monsoon to summertime precipitation in the region is limited. Streamwater and precipitation from the Yellow River source region and its surrounding areas demonstrate a best-fit second-order polynomial relationship between $\delta^{18}O$ and elevation over a 4600 m elevation range. A $\delta^{18}O$ elevation gradient of -1.6‰/km is also established and is consistent with the $\delta^{18}O$ elevation gradient of north and eastern plateau. The $\delta^{18}O$ values west of 98ºE do not show an elevation effect and paleoelevation reconstructions using such data may lead to higher uncertainties. The $\delta^{18}O$-elevation relationship of the Yellow River source region forms the basis of paleoelevation reconstructions on the eastern Tibetan Plateau. The results of this study also improve the understanding of hydrological cycle on the eastern Tibetan Plateau.

ACKNOWLEDGMENTS

The authors thank Buming Jiang for the help in field work and thank Ergang Lian for the measurement of stable isotope data. The authors thank the anonymous reviewers for their helpful comments. This research was supported by the Research Grants Council of the Hong

Kong Special Administrative Region, China (17304815), the National Natural Science Foundation of China (NSFC 91747204; 41625001), Guangdong Provincial Key Laboratory of Soil and Groundwater Pollution Control (No. 2017B030301012), and an AXA Research Fund Post-Doctoral Fellowship awarded to X.K. Additional support was provided by the Strategic Priority Research Program of Chinese Academy of Sciences (Grant XDA20060402).

REFERENCES

Araguás-Araguás, L., Froehlich, K., & Rozanski, K. (1998). Stable isotope composition of precipitation over southeast Asia. *Journal of Geophysical Research, 103,* 28721–28742.

Bershaw, J., Penny, S. M., & Garzione, C. N. (2012). Stable isotopes of modern water across the Himalaya and eastern Tibetan Plateau: Implications for estimates of paleoelevation and paleoclimate. *Journal of Geophysical Research*, *117,* D02110, doi:10.1029/2011JD016132.

Bolch, T., Kulkarni, A., Kääb, A., Huggel, C., Paul, F., Cogley, J. G., ... Stoffel, M. (2012). The state and fate of Himalayan glaciers. *Science, 336,* 310–314.

Caves, J. K., Winnick, M. J., Graham, S. A., Sjostrom, D. J., Mulch, A., & Chamberlain, C. P.

(2015). Role of the westerlies in Central Asia climate over the Cenozoic. *Earth and Planetary Science Letters*, *428*, 33–43.

Chen, B., Xu, X.-D., Yang, S., & Zhang, W. (2012). On the origin and destination of atmospheric moisture and air mass over the Tibetan Plateau. *Theoretical and Applied Climatology*, *110*, 423–435.

Cheng, G., & Wu, T. (2007). Responses of permafrost to climate change and their environmental significance, Qinghai-Tibet Plateau. *Journal of Geophysical Research*, *112*, F02S03, doi:10.1029/2006JF000631.

Clark, I. D., & Fritz, P. (1997). *Environmental Isotopes in Hydrogeology*. Boca Raton: CRC Press.

Craig, H. (1961). Isotopic variations in meteoric waters. *Science*, *133*, 1702–1073.

Curio, J., Maussion, F., & Scherer, D. (2015). A 12-year high-resolution climatology of atmospheric water transport over the Tibetan plateau. *Earth System Dynamics*, *6*, 109–124.

Currie, B. S., Rowley, D. B., & Tabor, N. J. (2005). Middle Miocene paleoaltimetry of southern Tibet: Implications for the role of mantle thickening and delamination in the Himalayan orogen. *Geology*, *33*, 181–184.

Cyr, A. J., Currie, B. S., & Rowley, D. B. (2005). Geochemical evaluation of Fenghuoshan Group lacustrine carbonates, north-central Tibet: Implications for the paleoaltimetry of the Eocene Tibetan Plateau. *Journal of Geology*, *113*, 517–533.

Dansgaard, W. (1964). Stable isotopes in precipitation. *Tellus*, *16*, 436–468.

Ding, L., Xu, Q., Zhang, L., Yang, D., Lai, Q., Huang, F., & Shi, E. (2009). Regional variation of river water oxygen isotope and empirical elevation prediction models in

Tibetan Plateau (in Chinese with English abstract). *Quaternary Sciences*, *29*, 1–12.

Feng, L., & Zhou, T. (2012). Water vapor transport for summer precipitation over the Tibetan Plateau: Multidata set analysis. *Journal of Geophysical Research*, *117*, D20114, doi:10.1029/2011JD017012.

Fritz, P. (1981). River waters. In: Gat, J.R., Gonfiantini, R. (Eds.), Stable Isotope Hydrology: Deuterium and Oxygen-18 in the Water Cycle, pp. 177–201. IAEA, Vienna, Austria.

Fröhlich, K., Gibson, J. J., & Aggarwal, P. K. (2001). Deuterium excess in precipitation and its climatological significance. Proceedings of the study of environmental change using isotope techniques, pp. 54–66.

Froehlich, K., Kralik, M., Papesch, W., Rank, D., Scheifinger, H., & Stichler, W. (2008). Deuterium excess in precipitation of Alpine regions-moisture recycling. *Isotopes in Environmental and Health Studies*, *44*, 61–70.

Garzione, C. N., Dettman, D. L., Quade, J., DeCelles, P. G., & Butler, R. F. (2000a). High times on the Tibetan Plateau: Paleoelevation of the Thakkhola graben, Nepal. *Geology*, *28*, 339–342.

Garzione, C. N., Quade, J., DeCelles, P. G., & English, N. B. (2000b). Predicting paleoelevation of Tibet and the Himalaya from $\delta^{18}O$ vs. altitude gradients in meteoric water across the Nepal Himalaya. *Earth and Planetary Science Letters*, *183*, 215–229.

Gat, J. R. (1996). Oxygen and hydrogen isotopes in the hydrologic cycle. *Annual Review of Earth and Planetary Sciences*, *24*, 225–262.

Gat, J. R., & Carmi, I. (1970). Evolution of the isotopic composition of atmospheric waters in the Mediterranean Sea area. *Journal of Geophysical Research*, *75*, 3039–3048.

Guan, H., Zhang, X., Skrzypek, G., Sun, Z., & Xu, X. (2013). Deuterium excess variations of rainfall events in a coastal area of South Australia and its relationship with synoptic weather systems and atmospheric moisture sources. *Journal of Geophysical Research Atmospheres*, *118*, 1123–1138.

Hoke, G. D., Jing, L.-Z., Hren, M. T., Wissink, G. K., & Garzione, C. N. (2014). Stable isotopes reveal high southeast Tibetan Plateau margin since the Paleogene. *Earth and Planetary Science Letters*, *394*, 270–278.

Hren, M. T., Bookhagen, B., Blisniuk, P. M., Booth, A. L., & Chamberlain, C. P. (2009). δ^{18}O and δD of streamwaters across the Himalaya and Tibetan Plateau: Implications for moisture sources and paleoelevation reconstructions. *Earth and Planetary Science Letters*, *288*, 20–32.

Hu, Y., Maskey, S., Uhlenbrook, S., & Zhao, H. (2011). Streamflow trends and climate linkages in the source region of the Yellow River, China. *Hydrological Processes*, *25*, 3399–3411.

Hu, Y., Maskey, S., & Uhlenbrook, S. (2013a). Downscaling daily precipitation over the Yellow River source region in China: a comparison of three statistical downscaling methods. *Theoretical and Applied Climatology*, *112*, 447–460.

Hu, Y., Maskey, S., & Uhlenbrook, S. (2013b). Expected changes in future temperature extremes and their elevation dependency over the Yellow River source region. *Hydrology and Earth System Sciences*, *17*, 2501–2514.

Johnson, K. R., & Ingram, B. L. (2004). Spatial and temporal variability in the stable isotope systematics of modern precipitation in China: implications for paleoclimate reconstructions.

Earth and Planetary Science Letters, *220*, 365–377.

Karim, A., & Veizer, J. (2002). Water balance of the Indus River Basin and moisture source in the Karakoram and western Himalayas: Implications from hydrogen and oxygen isotopes in river water. *Journal of Geophysical Research*, *107*, 4362, doi:10.1029/2000JD000253.

Kendall, C., & Coplen, T. B. (2001). Distribution of oxygen-18 and deuterium in river waters across the United States. *Hydrological Processes*, *15*, 1363–1393.

Koster, R. D., de Valpine, D. P., & Jouzel, J. (1993). Continental water recycling and $H_2{}^{18}O$ concentrations. *Geophysical Research Letters*, *20*, 2215–2218.

Kurita, N., & Yamada, H. (2008). The role of local moisture recycling evaluated using stable isotope data from over the middle of the Tibetan Plateau during the monsoon season. *Journal of Hydrometeorology*, *9*, 760–775.

Lan, Y., Kang, E., Ma, Q., Yang, W., & Yao, Z. (1999). Runoff forecast model for inflow to the Longyangxia Reservoir in the upper Yellow River basin during spring. *Journal of Glaciology and Geocryology*, *21*, 391–395.

Lan, Y., Zhao, G., Zhang, Y., Wen, J., Hu, X., Liu, J., ... Ma, J. (2010a). Response of runoff in the headwater region of the Yellow River to climate change and its sensitivity analysis. *Journal of Geographical Sciences*, *20*, 848–860.

Lan, Y., Zhao, G., Zhang, Y., Wen, J., Liu, J., & Hu, X. (2010b). Response of runoff in the source region of the Yellow River to climate warming. *Quaternary International*, *226*, 60–65.

Li, L., & Garzione, C. N. (2017). Spatial distribution and controlling factors of stable isotopes in meteoric waters on the Tibetan Plateau: Implications for paleoelevation reconstruction. *Earth and Planetary Science Letters*, *460*, 302–314.

Li, L., Zhang, G., Wang, Q., Shi, X., Dong, L., & Xu, W. (1999). Variation of surface water resource in Qinghai Province and its influent factors (in Chinese with English abstract). *Meteorological Monthly*, *25*, 11–15.

Liang, S., Ge, S., Wan, L., & Zhang, J. (2010). Can climate change cause the Yellow River to dry up?. *Water Resources Research*, *46*, W02505, doi:10.1029/2009WR007971.

Liu, Z., Tian, L., Chai, X., & Yao, T. (2008). A model-based determination of spatial variation of precipitation $\delta^{18}O$ over China. *Chemical Geology*, *249*, 203–212.

Luo, X., Kuang, X., Jiao, J. J., Liang, S., Mao, R., Zhang, X., & Li, H. (2018). Evaluation of lacustrine groundwater discharge, hydrologic partitioning, and nutrient budgets in a proglacial lake in the Qinghai–Tibet Plateau: using ^{222}Rn and stable isotopes. *Hydrology and Earth System Sciences*, *22*, 5579–5598.

Meng, F., Su, F., Yang, D., Tong, K., & Hao, Z. (2016). Impacts of recent climate change on the hydrology in the source region of the Yellow River basin. *Journal of Hydrology: Regional Studies*, *6*, 66–81.

Poage, M. A., & Chamberlain, C. P. (2001). Empirical relationships between elevation and the stable isotope composition of precipitation: considerations for studies of paleoelevation change. *American Journal of Science*, *301*, 1–15.

Quade, J., Garzione, C., & Eiler, J. (2007). Paleoelevation reconstruction using pedogenic carbonates. *Reviews in Mineralogy & Geochemistry*, *66*, 53–87.

Quade, J., Breecker, D. O., Daëron, M., & Eiler, J. (2011). The paleoaltimetry of Tibet: An isotopic perspective. *American Journal of Science*, *311*, 77–115.

Ren, W., Yao, T., Yang, X., & Joswiak, D. R. (2013). Implications of variations in $\delta^{18}O$ and $\delta^{2}H$ in precipitation at Madoi in the eastern Tibetan Plateau. *Quaternary International*, *313–314*, 56–61.

Ren, W., Yao, T., & Xie, S. (2017a). Key drivers controlling the stable isotopes in precipitation on the leeward side of the central Himalayas. *Atmospheric Research*, *189*, 134–140.

Ren, W., Yao, T., Xie, S., & He, Y. (2017b). Controls on the stable isotopes in precipitation and surface waters across the southeastern Tibetan Plateau. *Journal of Hydrology*, *545*, 276–287.

Rowley, D. B. (2007). Stable isotope-based paleoaltimetry: theory and validation. *Reviews in Mineralogy & Geochemistry*, *66*, 23–52.

Rowley, D. B., & Currie, B. S. (2006). Palaeo-altimetry of the late Eocene to Miocene Lunpola basin, central Tibet. *Nature*, *439*, 677–681.

Rowley, D. B., & Garzione, C. N. (2007). Stable isotope-based paleoaltimetry. *Annual Review of Earth and Planetary Sciences*, *35*, 463–508.

Rowley, D. B., Pierrehumbert, R. T., & Currie, B. S. (2001). A new approach to stable isotope-based paleoaltimetry: implications for paleoaltimetry and paleohypsometry of the High Himalaya since the Late Miocene. *Earth and Planetary Science Letters*, *188*, 253–268.

Rozanski, K., Araguás-Araguás, L., & Gonfiantini, R. (1993). Isotopic patterns in modern global precipitation, Geophysical Monograph 78, American Geophysical Union, 1–36.

Sato, Y., Ma, X., Xu, J., Matsuoka, M., Zheng, H., Liu, C., & Fukushima, Y. (2008). Analysis of long-term water balance in the source area of the Yellow River basin. *Hydrological Processes*, *22*, 1618–1629.

Siegenthaler, U., & Oeschger, H. (1980). Correlation of ^{18}O in precipitation with temperature and altitude. *Nature*, *285*, 314–317.

Song, C., Huang, B., Richards, K., Ke, L., & Phan, V. H. (2014). Accelerated lake expansion on the Tibetan Plateau in the 2000s: Induced by glacial melting or other processes?. *Water Resources Research*, *50*, 3170–3186.

Tian, L., Masson-Delmotte, V., Stievenard, M., Yao, T., & Jouzel, J. (2001a). Tibetan Plateau summer monsoon northward extent revealed by measurements of water stable isotopes. *Journal of Geophysical Research*, *106*, 28081–28088.

Tian, L., Yao, T., Sun, W., Stievenard, M., & Jouzel, J. (2001b). Relationship between δD and δ^{18}O in precipitation on north and south of the Tibetan Plateau and moisture recycling. *Science in China (D)*, *44*, 789–796.

Tian, L., Yao, T., Schuster, P. F., White, J. W. C., Ichiyanagi, K., Pendall, E., ... Yu, W. (2003). Oxygen-18 concentrations in recent precipitation and ice cores on the Tibetan Plateau. *Journal of Geophysical Research*, *108*, 4293, doi:10.1029/2002JD002173.

Tian, L., Yao, T., MacClune, K., White, J. W. C., Schilla, A., Vaughn, B., ... Ichiyanagi, K. (2007). Stable isotopic variations in west China: A consideration of moisture sources. *Journal of Geophysical Research*, *112*, D10112, doi:10.1029/2006JD007718.

Tian, L., Ma, L., Yu, W., Liu, Z., Yin, C., Zhao, Z., ... Wang, Y. (2008). Seasonal variations of stable isotope in precipitation and moisture transport at Yushu, eastern Tibetan Plateau. *Science in China (D)*, *51*, 1121–1128.

Wang, Y., Wang, X., Li, C., Wu, F., & Yang, Z. (2015). Spatiotemporal analysis of temperature trends under climate change in the source region of the Yellow River, China. *Theoretical and Applied Climatology, 119*, 123–133.

Weynell, M., Wiechert, U., & Zhang, C. (2016). Chemical and isotopic (O, H, C) composition of surface waters in the catchment of Lake Donggi Cona (NW China) and implications for paleoenvironmental reconstructions. *Chemical Geology, 435*, 92–107.

Xu, Q., Hoke, G. D., Liu-Zeng, J., Ding, L., Wang, W., & Yang, Y. (2014). Stable isotopes of surface water across the Longmenshan margin of the eastern Tibetan Plateau. *Geochemistry, Geophysics, Geosystems*, *15*, 3416–3429.

Yang, J., Ding, Y., Chen, R., Liu, S., & Lu, A. (2003). Causes of glacier change in the source regions of the Yangtze and Yellow rivers on the Tibetan Plateau. *Journal of Glaciology*, *49,* 539–546.

Yang, J., Ding, Y., & Chen, R. (2007a). Climatic causes of ecological and environmental variations in the source regions of the Yangtze and Yellow Rivers of China. *Environmental Geology*, *53*, 113–121.

Yang, M., Yao, T., Wang, H., Tian, L., & Gou, X. (2006). Estimating the criterion for determining water vapour sources of summer precipitation on the northern Tibetan Plateau. *Hydrological Processes*, *20*, 505–513.

Yang, M., Yao, T., Gou, X., & Tang, H., (2007b). Water recycling between the land surface and atmosphere on the Northern Tibetan Plateau-A case study at flat observation sites. *Arctic, Antarctic, and Alpine Research*, *39*, 694–698.

Yao, T., Zhou, H., & Yang, X. (2009). Indian monsoon influences altitude effect of $\delta^{18}O$ in precipitation/river water on the Tibetan Plateau. *Chinese Science Bulletin*, *54*, 2724–2731.

Yao, T., Thompson, L., Yang, W., Yu, W., Gao, Y., Guo, X., ... Joswiak, D. (2012). Different glacier status with atmospheric circulations in Tibetan Plateau and surroundings. *Nature Climate Change*, *2*, 663–667.

Yao, T., Masson-Delmotte, V., Gao, J., Yu, W., Yang, X., Risi, C., ... Hou, S. (2013). A review of climatic controls on $\delta^{18}O$ in precipitation over the Tibetan Plateau: Observations and simulations. *Reviews of Geophysics*, *51*, 525–548.

You, Q., Min, J., Zhang, W., Pepin, N., & Kang, S. (2015). Comparison of multiple datasets with gridded precipitation observations over the Tibetan Plateau. *Climate Dynamics*, *45*, 791–806.

Yurtsever, Y., & Gat, J. (1981). Atmospheric waters. In: Gat, J.R., Gonfiantini, R. (Eds.), Stable Isotope Hydrology: Deuterium and Oxygen-18 in the Water Cycle, pp. 103–142. IAEA, Vienna, Austria.

Zhang, J., Li, G., & Liang, S. (2012). The response of river discharge to climate fluctuations in the source region of the Yellow River. *Environmental Earth Sciences*, *66*, 1505–1512.

Zhang, L., Su, F., Yang, D., Hao, Z., & Tong, K. (2013). Discharge regime and simulation for the upstream of major rivers over Tibetan Plateau. *Journal of Geophysical Research Atmospheres*, *118*, 8500–8518.

Zheng, H., Zhang, L., Liu, C., Shao, Q., & Fukushima, Y. (2007). Changes in stream flow regime in headwater catchments of the Yellow River basin since the 1950s. *Hydrological Processes*, *21*, 886–893.

Zheng, H., Zhang, L., Zhu, R., Liu, C., Sato, Y. & Fukushima, Y. (2009). Responses of streamflow to climate and land surface change in the headwaters of the Yellow River Basin. *Water Resources Research*, *45*, W00A19, doi:10.1029/2007WR006665.

Zhou, D., & Huang, R. (2012). Response of water budget to recent climatic changes in the source region of the Yellow River. *Chinese Science Bulletin*, *57*, 2155–2162.

Appendix A

TABLE 1

Isotopic compositions of surface water and groundwater across the Yellow River source region.

Sample	Date sampled	Latitude	Longitude	Sample elevation (m)	$\delta^{18}O$ (‰)	$\delta^{2}H$ (‰)	d-excess	Description
Tributaries								
YGZ-1	Aug 30	35.0848	96.5580	4324	-9.1	-65.4	7.4	Yueguzonglie Qu
YGZ-2	Aug 30	35.0801	96.6067	4321	-8.7	-66.9	2.5	Tributary
YGZ-3	Aug 30	35.0788	96.8593	4338	-10.3	-73.1	9.3	Tributary
YGZ-4	Aug 30	35.0627	96.9131	4347	-10.1	-70.8	9.9	Tributary
ZLH-10	Aug 30	35.0375	97.4007	4320	-9.6	-68.1	8.6	Tributary
ZLH-11	Aug 30	35.0197	97.5758	4297	-10.6	-80.9	3.6	Tributary
DUQ-2	Aug 31	34.7566	97.2484	4320	-9.3	-66.2	8.4	Duo Qu
DUQ-3	Aug 31	34.8078	97.4371	4284	-5.8	-46.5	-0.4	Duo Qu
DUQ-1	Aug 31	34.6861	97.3202	4351	-11.4	-77.2	13.8	Tributary
HHX-1	Sep 01	34.6015	98.2673	4211	-10.2	-72.5	8.9	Re Qu
BMH-1	Sep 01	34.2255	98.8977	4164	-11.2	-82.3	7.7	Baima Qu
XQ-1	Sep 01	34.1011	99.0186	4130	-11.6	-85.4	7.3	Xia Qu
CMH-2	Aug 27	34.6940	99.1113	4490	-12.2	-81.4	16.3	Tributary
CMH-1	Aug 27	34.5094	99.1584	4349	-12.3	-82.9	15.2	Tributary
YY-1	Aug 27	34.2751	99.1940	4214	-11.7	-87.0	7.0	Tributary
DR-18	Aug 27	33.8177	99.7055	3933	-11.8	-86.0	8.4	Tributary
KQ-1	Aug 20	33.9485	99.0715	4117	-13.5	-91.9	15.8	Ke Qu
DR-2	Aug 20	33.7687	99.6595	3992	-13.3	-95.7	10.6	Dari River
DR-8	Aug 26	33.7603	99.6759	3938	-12.0	-90.5	5.2	Tributary
DR-13	Aug 26	33.5590	100.1659	3880	-12.6	-93.5	7.6	Tributary
DR-15	Aug 26	33.6956	99.9227	3934	-12.3	-87.3	11.0	Tributary
DR-16	Aug 26	33.7231	99.8745	3953	-12.0	-86.0	10.2	Tributary
DR-17	Aug 26	33.7565	99.6438	3961	-11.8	-83.8	10.8	Tributary
XKQ-1	Sep 02	33.9700	99.9060	3995	-12.2	-86.5	11.5	Xike Qu
GAD-1	Aug 25	33.8611	100.0641	3916	-11.5	-83.6	8.7	Xike Qu
XZK-1	Aug 25	34.1069	100.6554	3791	-11.2	-80.3	9.0	Tributary
MUL-1	Aug 25	33.8445	101.1593	3609	-10.9	-80.5	6.8	Tributary
XN-11	Aug 24	33.4293	101.0932	3974	-12.4	-87.9	11.0	Nige Qu tributary
XN-12	Aug 24	33.4443	101.0884	3955	-12.5	-89.0	11.1	Nige Qu tributary
SKH-1	Aug 25	33.4652	101.4961	3610	-11.4	-82.2	9.0	Shake River

QZ-1	Aug 19	34.1504	100.1509	4066	-11.8	-84.5	10.3	Dongke Qu
GQH-1	Sep 02	34.4317	100.2633	3757	-11.7	-78.2	15.4	Ge Qu
WMH-1	Sep 02	34.5483	100.5360	3509	-10.9	-73.1	14.0	Tributary
WMH-2	Sep 02	34.6174	100.5689	3352	-10.8	-73.0	13.5	Tributary
SQQ-2	Sep 02	34.8972	100.8794	3752	-10.3	-70.0	12.2	Saiqian Qu
SQQ-1	Sep 02	34.7463	100.8098	3295	-9.9	-68.6	10.9	Saiqian Qu
TD-1	Aug 18	35.2565	100.5640	3052	-9.8	-71.6	7.0	Ba Qu
ML-1	Aug 18	35.5981	100.7453	3055	-8.7	-65.7	4.0	Mang Qu
Mainstream								
SSY-1	Aug 28	34.8233	97.4463	4278	-3.6	-34.3	-5.1	Mainstream
MAD-1	Sep 01	34.8847	98.1705	4217	-3.9	-37.5	-6.2	Mainstream
HHX-2	Sep 01	34.4680	98.4645	4187	-4.4	-45.1	-9.9	Mainstream
THT-4	Sep 01	33.9651	99.0648	4102	-7.4	-58.7	0.9	Mainstream
TH-1	Aug 20	33.9198	99.1001	4100	-9.6	-73.5	3.6	Mainstream
DR-1	Aug 20	33.7687	99.6595	3945	-10.2	-76.1	5.8	Mainstream
DR-3	Aug 20	33.8223	99.2062	4059	-9.5	-72.1	3.7	Mainstream
DR-4	Aug 20	33.7323	99.3066	4032	-10.1	-76.4	4.8	Mainstream
DR-5	Aug 20	33.7515	99.5758	3966	-10.7	-80.2	5.0	Mainstream
DR-9	Aug 26	33.8016	99.7456	3943	-10.0	-77.0	3.0	Mainstream
DR-10	Aug 26	33.7545	99.8462	3926	-9.9	-77.0	2.2	Mainstream
DR-11	Aug 26	33.6796	99.9438	3905	-10.5	-77.7	6.5	Mainstream
DR-12	Aug 26	33.6198	100.2392	3867	-10.5	-78.3	5.7	Mainstream
DR-14	Aug 26	33.9238	100.0833	3888	-10.2	-77.0	4.5	Mainstream
GAL-2	Aug 25	33.8388	100.5131	3766	-10.2	-78.8	2.8	Mainstream
GAL-1	Aug 25	33.9275	100.6815	3720	-10.2	-77.9	3.5	Mainstream
ZLX-1	Aug 25	33.8626	100.8331	3694	-10.4	-79.5	4.1	Mainstream
MET-2	Aug 25	33.9182	100.7876	3709	-11.0	-79.4	8.4	Mainstream
MET-1	Aug 25	33.7946	101.0298	3634	-10.9	-80.5	6.8	Mainstream
MXH-1	Aug 25	33.7594	101.2252	3581	-10.6	-79.5	5.2	Mainstream
JZ-3	Aug 25	33.6977	101.3398	3559	-10.9	-79.3	8.1	Mainstream
JZ-2	Aug 25	33.6874	101.4547	3537	-11.1	-79.1	10.0	Mainstream
JZ-1	Aug 24	33.6796	101.5548	3522	-11.2	-80.7	8.9	Mainstream
MQ-1	Aug 24	33.9583	102.0809	3411	-11.3	-82.3	8.2	Mainstream
LJ-1	Aug 19	34.6735	100.6470	3078	-10.5	-75.9	8.5	Mainstream
XH-1	Aug 19	35.3361	100.2044	2705	-10.7	-78.1	7.9	Mainstream
LYX-1	Sep 03	35.6801	100.2519	2611	-11.1	-77.5	11.4	Mainstream
LXW-1	Aug 18	36.0694	101.2468	2231	-11.0	-79.7	8.7	Mainstream
GD-1	Aug 18	36.0603	101.4522	2186	-10.6	-79.1	6.1	Mainstream
Lakes								
ZLH-9	Aug 30	35.0142	97.2829	4295	-3.2	-31.8	-6.4	Zhaling Lake
ZLH-3	Aug 28	34.8801	97.1689	4298	-2.9	-30.1	-7.1	Zhaling Lake
ZLH-2	Aug 28	34.8766	97.1699	4288	-2.9	-30.5	-6.9	Zhaling Lake
ZLH-4	Aug 28	34.8606	97.1921	4294	-3.0	-30.0	-6.2	Zhaling Lake
ZLH-5	Aug 28	34.8387	97.2307	4296	-2.8	-29.1	-6.9	Zhaling Lake

ZLH-1	Aug 28	34.8283	97.2679	4283	-2.9	-30.2	-7.2	Zhaling Lake
ZLH-6	Aug 28	34.8216	97.2799	4294	-2.8	-29.1	-6.8	Zhaling Lake
ELH-4	Aug 31	34.8668	97.5038	4276	-2.4	-29.4	-10.2	Eling Lake
ELH-5	Aug 31	34.9095	97.5724	4276	-4.1	-38.0	-5.5	Eling Lake
ELH-3	Aug 31	34.9462	97.5954	4274	-4.1	-38.3	-5.5	Eling Lake
ELH-2	Aug 31	35.0596	97.7012	4272	-4.0	-38.1	-5.7	Eling Lake
ELH-1	Aug 31	35.0868	97.7631	4271	-3.7	-37.3	-7.5	Eling Lake
BS-1	Aug 31	35.1025	97.9130	4272	-3.8	-36.1	-5.7	Reservoir
CMC-1	Aug 28	34.8217	97.3651	4292	-1.7	-26.7	-13.5	Chamu Co
XXH-1	Sep 01	34.8492	98.1312	4218	-1.4	-24.7	-13.4	Xingxinghai
XXH-2	Sep 01	34.8516	98.1311	4217	-2.1	-28.4	-11.9	Xingxinghai
RGM-1	Sep 01	34.3049	98.6378	4175	-0.7	-21.7	-16.2	Gangnagema Co
YN-3	Aug 23	33.3347	101.1144	4021	-12.9	-91.8	11.4	Ximen Co
YN-2	Aug 23	33.3367	101.1147	4021	-13.4	-93.2	14.3	Ximen Co
YN-1	Aug 23	33.3509	101.1011	4024	-13.3	-91.9	14.4	Ximen Co
YN-4	Aug 23	33.3563	101.1014	4023	-13.1	-91.4	13.1	Ximen Co
XN-1	Aug 22	33.3748	101.0946	4024	-12.1	-87.8	9.4	Ximen Co
XN-2	Aug 22	33.3621	101.0937	4011	-12.4	-88.7	10.1	Ximen Co
XN-3	Aug 22	33.3206	101.0539	4013	-12.2	-87.8	9.6	Ximen Co
XN-4	Aug 22	33.3868	101.1015	4019	-12.3	-87.6	11.2	Ximen Co
XN-5	Aug 22	33.3454	101.5172	4019	-12.1	-87.8	9.0	Ximen Co
XN-6	Aug 23	33.3601	101.1006	4023	-12.3	-89.0	9.4	Ximen Co
XN-7	Aug 23	33.3689	101.1042	4023	-12.2	-88.1	9.4	Ximen Co
XN-8	Aug 23	33.3833	101.1110	4025	-12.1	-87.5	9.4	Ximen Co
XN-9	Aug 23	33.3929	101.1128	4025	-12.2	-87.6	9.8	Ximen Co
XN-10	Aug 23	33.3972	101.1069	4023	-12.2	-87.1	10.3	Ximen Co
Groundwater								
ELW-1	Aug 31	34.9080	97.5669	4289	-11.9	-86.0	9.5	Eling Lake well
ELW-2	Aug 31	34.9085	97.5678	4288	-12.1	-89.1	7.8	Eling Lake well
ELW-3	Aug 31	34.9082	97.5668	4291	-12.0	-89.2	7.0	Eling Lake well
ZLJ-1	Aug 29	35.0852	97.9091	4264	-10.5	-80.1	4.0	Zhaling Lake well
XNP-8	Aug 22	33.3916	101.1033	4018	-12.0	-86.7	9.2	Ximen Co
XNP-7	Aug 22	33.3927	101.1030	4018	-12.2	-85.5	11.8	Ximen Co
XNP-6	Aug 22	33.3936	101.1031	4018	-12.1	-85.1	11.6	Ximen Co
XNP-5	Aug 22	33.3943	101.1048	4018	-11.7	-82.9	10.6	Ximen Co
XNP-4	Aug 22	33.3938	101.1059	4018	-11.8	-84.1	10.4	Ximen Co
XNP-3	Aug 22	33.3943	101.1069	4018	-11.8	-84.4	10.4	Ximen Co
XNP-2	Aug 22	33.3952	101.1072	4018	-12.7	-91.3	10.0	Ximen Co
XNP-1	Aug 22	33.3963	101.1071	4018	-11.5	-83.7	8.5	Ximen Co
MQP-1	Aug 24	33.9583	102.0809	3411	-11.9	-87.1	8.1	Maqu

TABLE 2

Elevation effect for the tributaries.

Sample	$\delta^{18}O$	Basin mean elevation (m)	Predicted[a]	Predicted[b]	Difference[a]	Difference[b]
DUQ-1	-11.4	4495	4135	4074	360	421
BMH-1	-11.2	4347	4082	3994	265	353
XQ-1	-11.6	4369	4219	4204	150	165
CMH-2	-12.2	4544	4451	4594	93	-50
CMH-1	-12.3	4544	4468	4625	76	-81
YY-1	-11.7	4544	4280	4303	264	241
KQ-1	-13.5	4557	4830	5368	-272	-811
DR-18	-11.8	4299	4299	4334	0	-35
DR-8	-12.0	4246	4362	4440	-116	-194
DR-13	-12.6	4458	4587	4848	-129	-390
DR-15	-12.3	4570	4472	4631	98	-62
DR-16	-12.0	4236	4380	4470	-144	-234
DR-17	-11.8	4224	4311	4353	-87	-129
XKQ-1	-12.2	4356	4461	4613	-105	-257
GAD-1	-11.5	4356	4203	4179	153	176
XZK-1	-11.2	4317	4049	3944	268	373
MUL-1	-10.9	4094	3937	3783	156	311
XN-11	-12.4	4226	4499	4681	-272	-455
XN-12	-12.5	4226	4549	4774	-322	-548
SKH-1	-11.4	3935	4144	4087	-208	-152
QZ-1	-11.8	4317	4318	4365	-1	-48
GQH-1	-11.7	4152	4261	4272	-110	-121
WMH-1	-10.9	3987	3929	3771	58	216
WMH-2	-10.8	3987	3893	3721	94	266
SQQ-2	-10.3	3752	3643	3387	109	365
SQQ-1	-9.9	3752	3480	3183	272	569
TD-1	-9.8	3623	3419	3108	204	515
ML-1	-8.7	3389	2812	2427	577	962

[a]Predicted elevation using the second order least squares polynomial relationship.

[b]Predicted elevation using sea level $\delta^{18}O$=-4.8‰ and an -0.16‰/100 m $\delta^{18}O$ elevation gradient.

Difference equals to basin mean elevation minus predicted elevation.

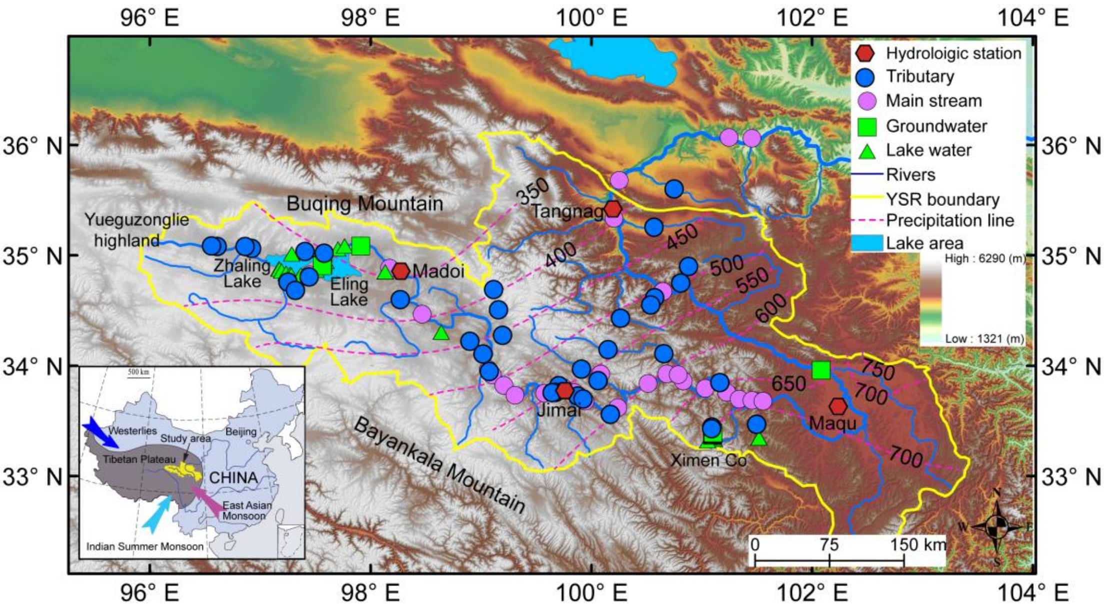

Figure 1 Location and topography of the Yellow River source region and locations of the sampling sites. Mean annual precipitation contours (mm) are also presented according to Meng et al. (2016).

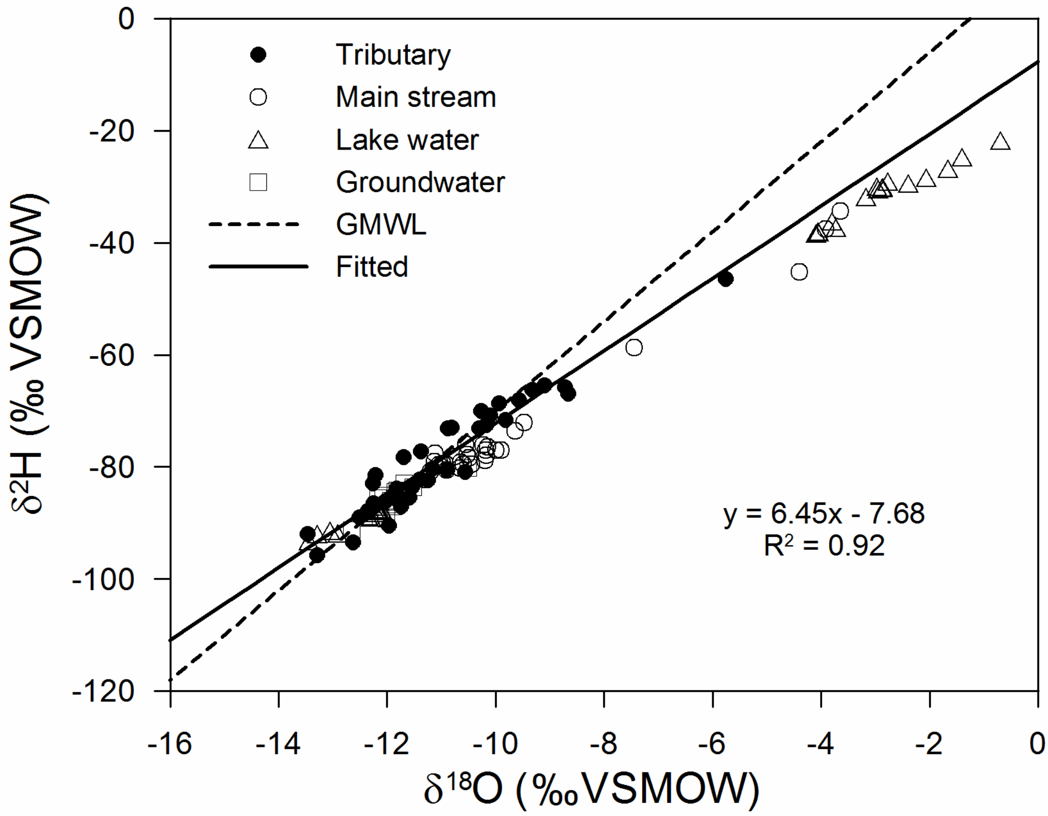

Figure 2 The relationship between δ^2H and δ^{18}O of stream water across the Yellow River source region. Lake water and groundwater are also shown. The dashed line is the global meteoric water line (GMWL).

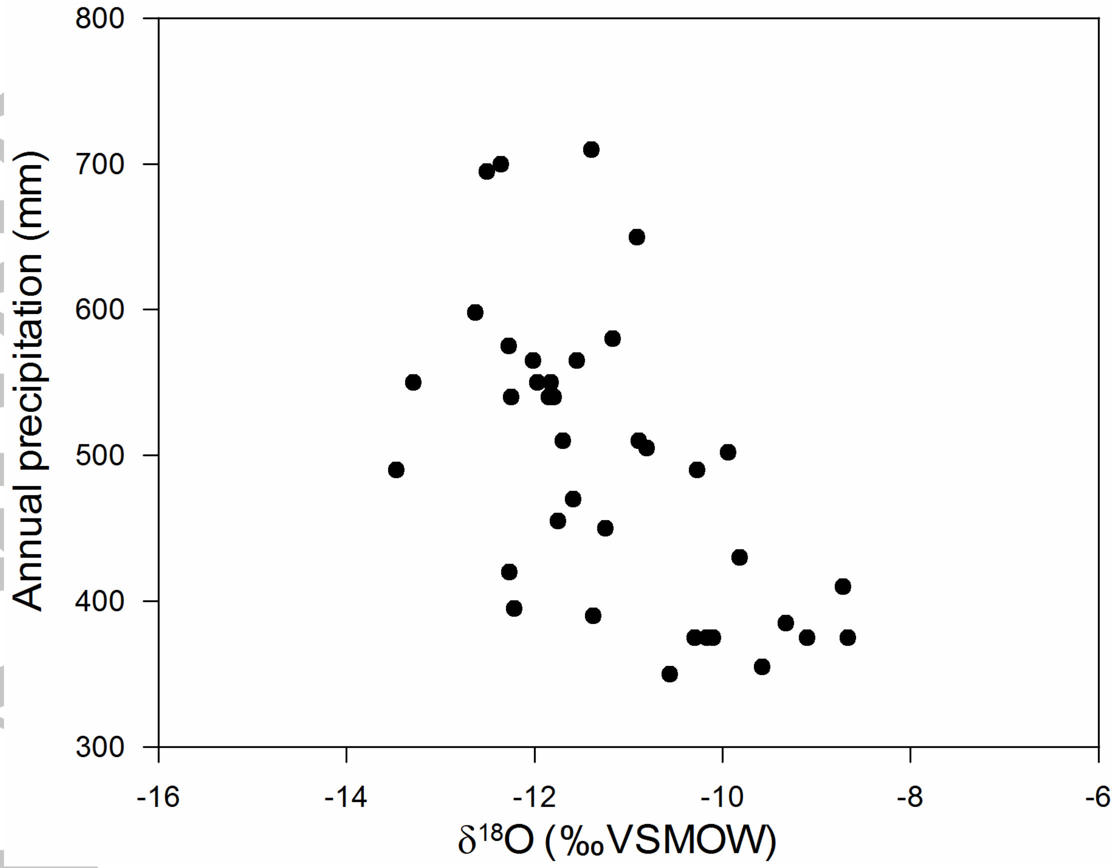

Figure 3 δ^{18}O of tributary waters as a function of total annual precipitation.

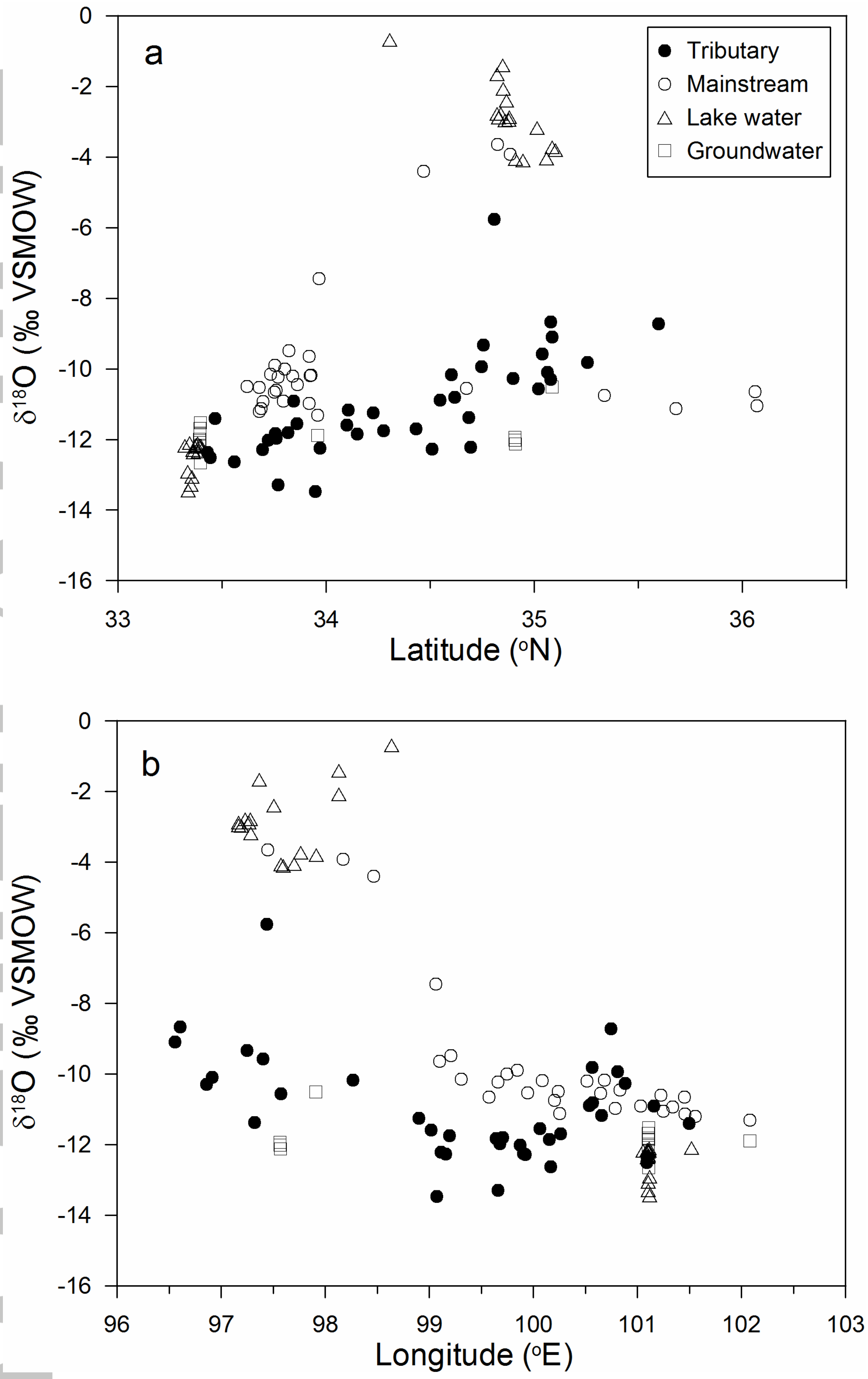

Figure 4 $\delta^{18}O$ of stream water, lake water, and groundwater as a function of latitude (a) and longitude (b).

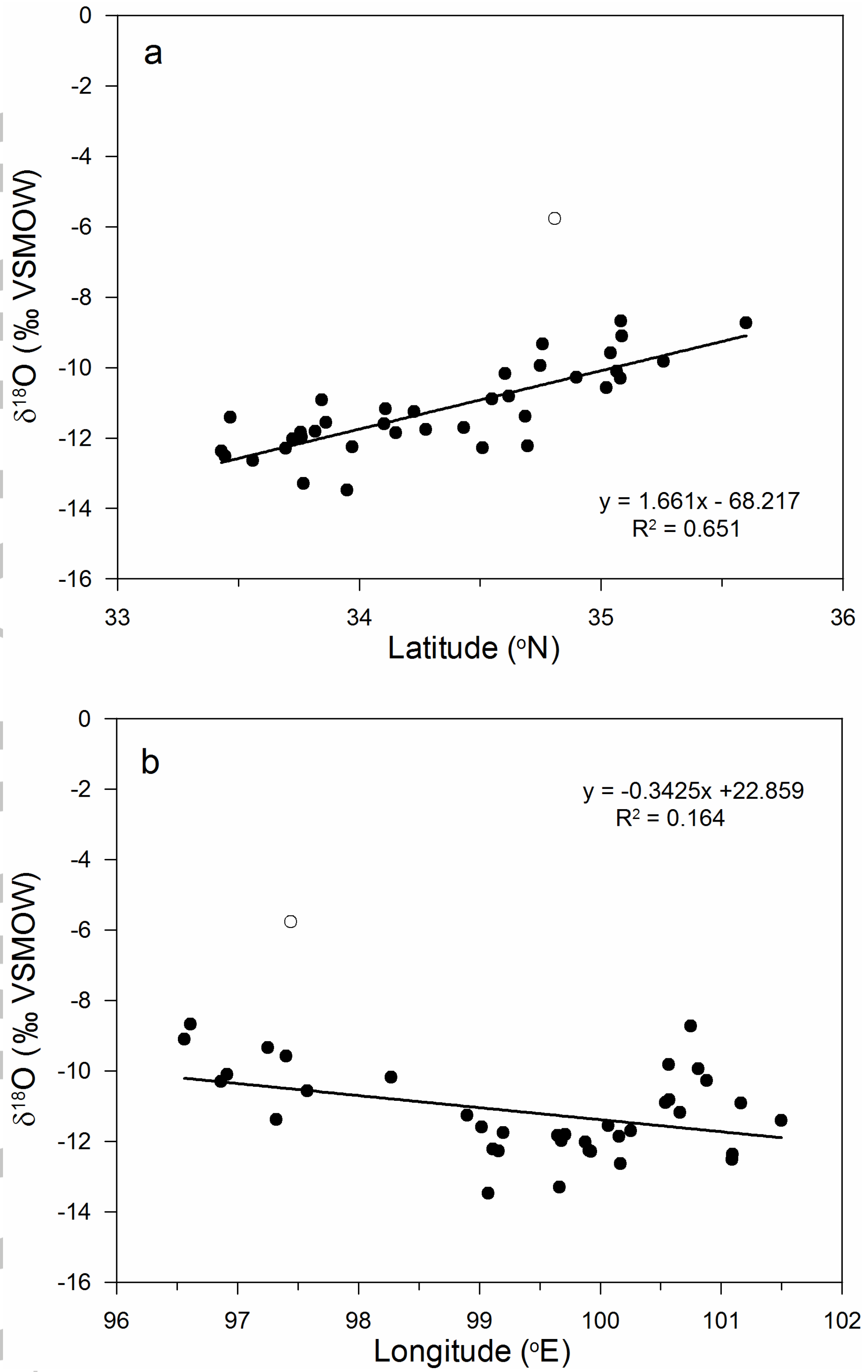

Figure 5 δ^{18}O of the tributaries as a function of latitude (a) and longitude (b). The sample represented by an open circle (DUQ-3) was not included in the regression as its abnormally high value does not seem possibly to represent regional trends.

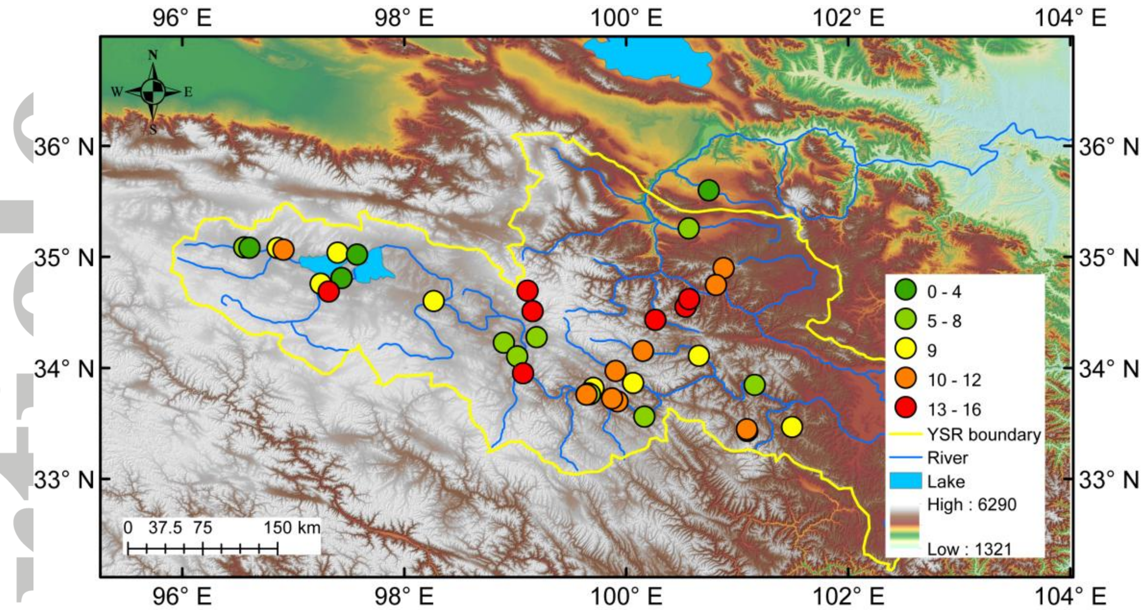

Figure 6 Distributions of tributary $\delta^{18}O$ values in the Yellow River source region.

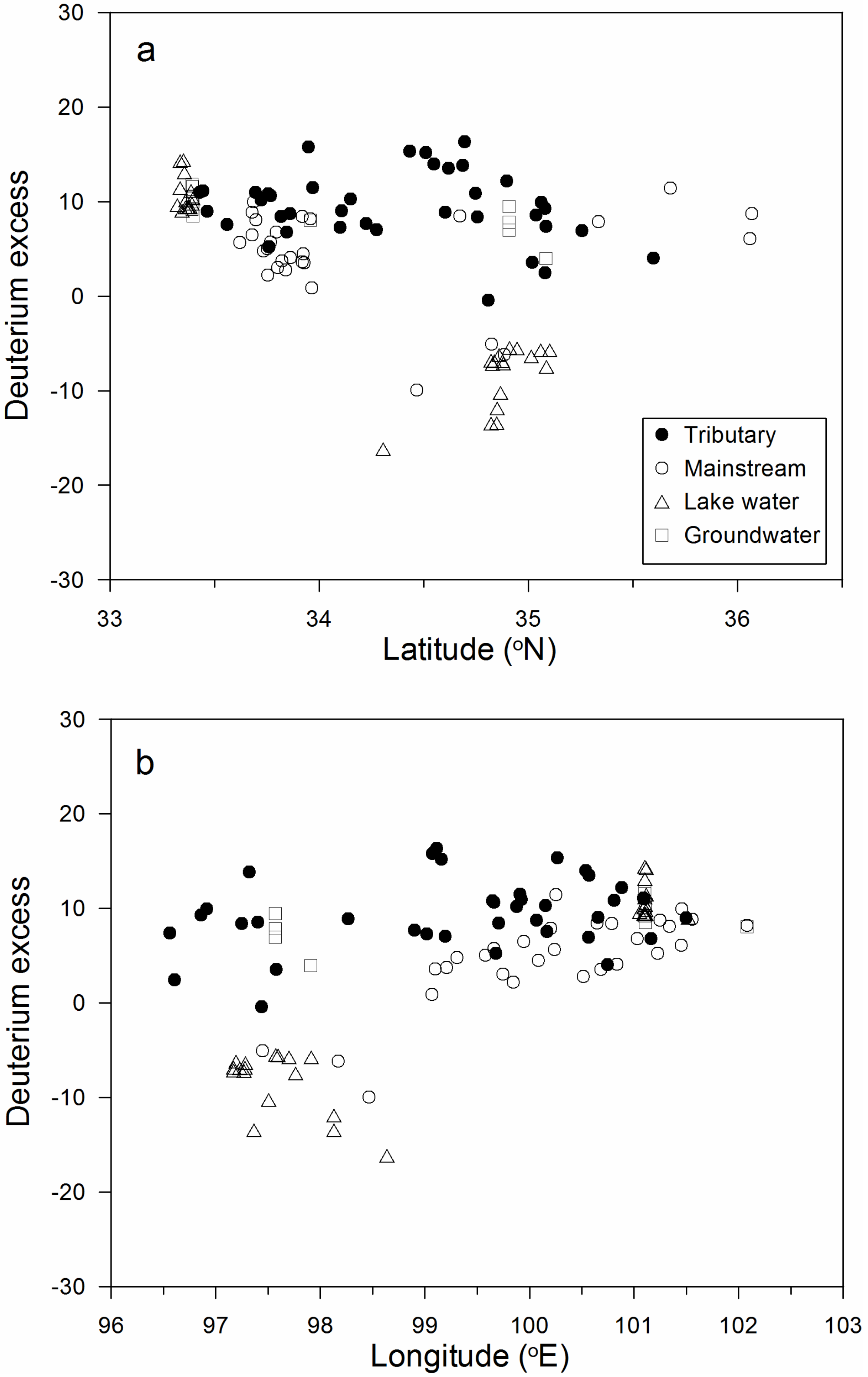

Figure 7 Deuterium excess of stream water, lake water, groundwater, and precipitation as a function of latitude (a) and longitude (b).

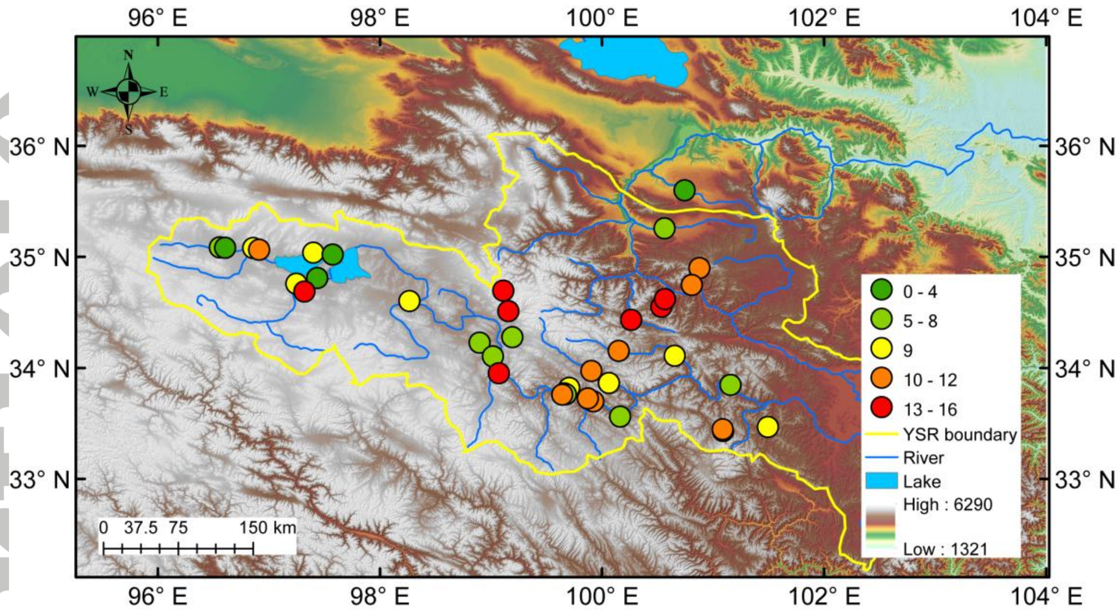

Figure 8 Distributions of d-excess of the tributaries in the Yellow River source region.

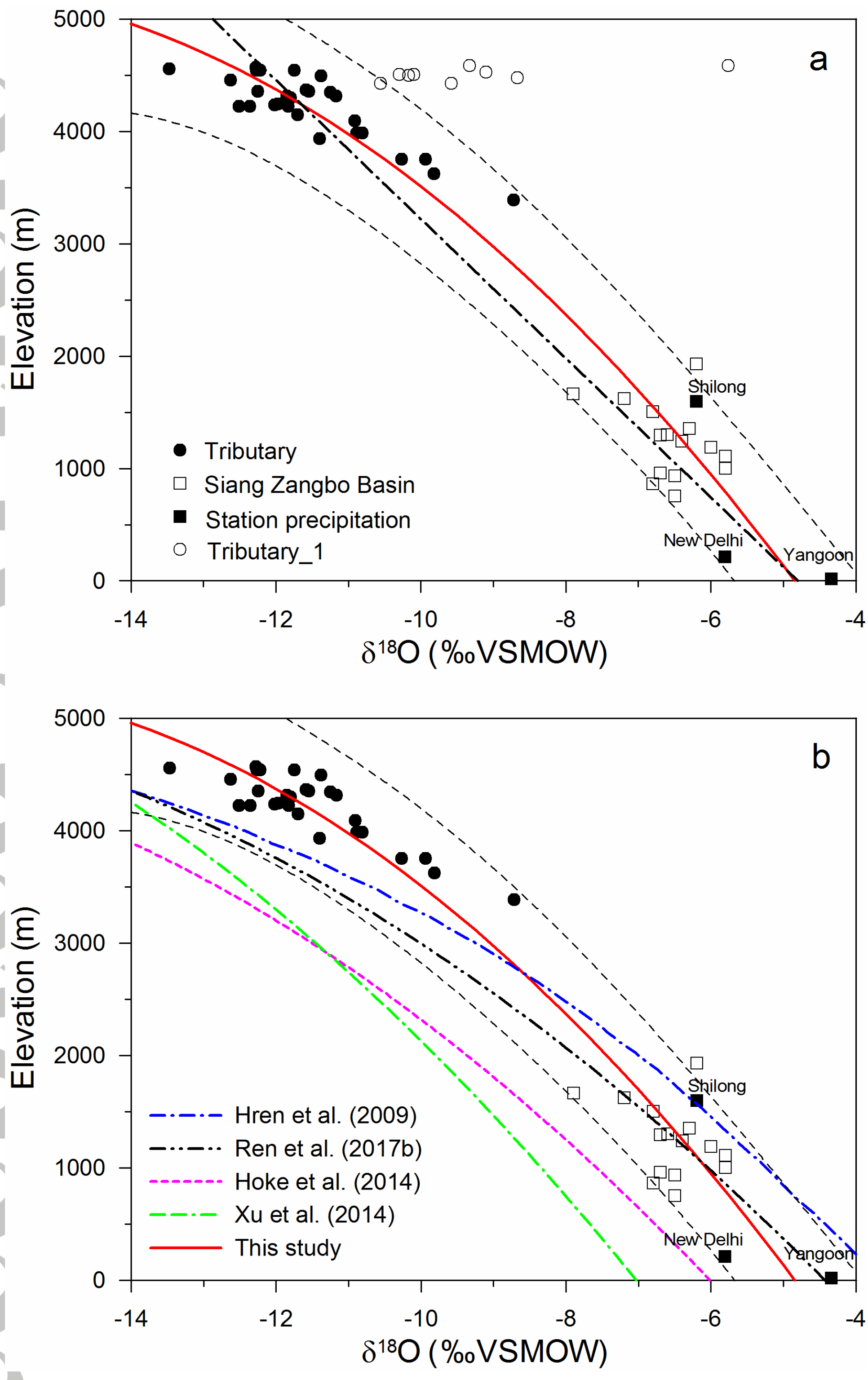

Figure 9 δ^{18}O-elevation relationships for the Yellow River source region and surrounding areas. (a) δ^{18}O-elevation relationships for the Yellow River source region, Siang Zangbo Basin, and GNIP stations in the surrounding areas. The 95% confidence interval on the regression (dashed lines) is shown for comparison. The δ^{18}O elevation gradient by linear

regression of -1.6‰/km (with a starting $\delta^{18}O$=-4.8‰) for the region is also shown. The nine samples denoted by open circles were not included in the least squares polynomial fit. (b) Comparison of different $\delta^{18}O$-elevation relationships on the southeastern and eastern Tibetan Plateau.